Geology

Effects of topography on pyroclastic density current runout and formation of coignimbrites

Benjamin J. Andrews and Michael Manga

Geology 2011;39;1099-1102
doi: 10.1130/G32226.1

Notes

Effects of topography on pyroclastic density current runout and formation of coignimbrites

Benjamin J. Andrews[1] and Michael Manga[2]
[1]Department of Mineral Sciences, National Museum of Natural History, Smithsonian Institution, 1000 Constitution Avenue Northwest, Washington, D.C. 20004, USA
[2]Department of Earth and Planetary Science, University of California–Berkeley, 307 McCone Hall, Berkeley, California 94720, USA

ABSTRACT

Laboratory experiments of dilute mixtures of warm talc powder in air simulate dilute pyroclastic density currents (PDCs) and show the effects of topography on current runout, buoyancy reversal, and liftoff into buoyant plumes. The densimetric and thermal Richardson, Froude, Stokes, and settling numbers for our experiments match those of natural PDCs. The laboratory currents are fully turbulent, although the experiments have lower Reynolds numbers than PDCs. In sum, our experiments are dynamically similar to natural currents. Comparisons of currents traversing flat topography or encountering barriers show that runout distance is not significantly reduced for currents that traverse barriers with height <1.5 times the current thickness, but currents do not pass taller barriers. Buoyancy reversals occur in most currents, resulting in liftoff and generation of a buoyant plume. Liftoff occurs near the maximum runout distance for currents traveling over flat topography, but is focused near or above barriers for currents that encounter barriers. Notably, plume formation above barriers can result in reversal of flow direction downstream of the obstruction as portions of the current flow back and feed the rising plume.

INTRODUCTION

Pyroclastic density currents (PDCs) present substantial hazards because of their high speeds, high temperatures, long runout distances, and ability to generate buoyant plumes that inject ash into the atmosphere. Because the dilute parts of currents are highly inflated and have thicknesses in excess of hundreds of meters, PDCs are very mobile and can transit substantial topographic barriers. As examples, currents depositing the Campanian Ignimbrite overtopped the 685–1000-m-high ridge of the Sorrento Peninsula, Italy (Fisher et al., 1993), PDCs from Fisher Caldera crossed the 500–700-m-high Tugamak Range (Alaska) during the 9400 ^{14}C yr B.P. eruption (Miller and Smith, 1977; Gardner et al., 2007), PDCs generated during the 18 May 1980 Mount St. Helens (Washington State) eruption overtopped the >200-m-tall Johnston Ridge (Criswell, 1987; Bursik et al., 1998), and in 1991 currents at Unzen (Japan) traversed barriers with >100 m of relief (Fujii and Nakada, 1999). Systematic studies of the effects of topography on PDC behavior are limited (e.g., Woods, et al., 1998; Bursik and Woods, 2000; Doronzo et al., 2010), particularly with regard to buoyant plume (coignimbrite) generation.

PDCs move because of density contrasts between the currents and the atmosphere, and, topographic effects aside, their behavior is largely controlled by the evolution of current density and thickness. During transport, the current density decreases as particles sediment and ambient fluid is entrained, heated, and expands (Woods and Kienle, 1994; Bursik and Woods, 1996); alternatively, current density can increase as the substrate is eroded and entrained (Calder et al., 2000). Unlike turbidity currents and powder snow avalanches, PDCs are hot (up to magmatic temperatures), and thus the thermal expansion of entrained air can result in buoyancy reversal and the generation of a coignimbrite plume (Woods and Kienle, 1994). Such plumes can be generated from comparatively small eruptions, e.g., the 1990 eruption of Redoubt, Alaska (Woods and Kienle, 1994), and are responsible for the dispersal of the majority of the airfall tephra in very large eruptions (Bursik and Woods, 1996; Wilson, 2008).

Interaction with topography will affect PDCs in several ways. Because energy is expended to traverse ridges, interactions with topography may reduce runout distance. Interaction with topography likely increases air entrainment and may increase sedimentation rates, resulting in reduced current density, earlier buoyancy reversal, and more vigorous coignimbrite plume generation.

Scaled laboratory experiments provide a means of studying the effects of temperature, discharge rate, current thickness, particle concentration, and topography on current behavior. As many aspects of PDC behavior are affected by thermal expansion, it is critical to model these currents in a compressible fluid (e.g., Dufek and Bergantz, 2007; Doronzo et al., 2010). Our experiments focus on understanding the dilute portions of PDCs by modeling them with heated, fine-grained powder suspended in air. Our experiments are properly scaled with respect to bulk, turbulent, and thermal properties of the currents and sediment, and thus these laboratory currents are dynamically similar to natural dilute PDCs.

METHODS

We used heated 20 mm talc powder to generate dilute particle-laden gravity currents in air within a 6.5 × 1.8 × 0.6 m acrylic tank. Details of the experimental apparatus, procedures, and data processing are described in the GSA Data Repository[1]. Briefly, powder is heated to the desired temperature (30–100 °C) in an oven, loaded onto a conveyor belt, and fed into the tank at a known mass discharge. Experiments are recorded with four high-definition video cameras, and we correct for lens distortions and lighting effects in each frame with postprocessing.

Experiments were conducted with and without topographic barriers. Barriers were built of 1.9-cm-thick plywood oriented vertically (on edge) with heights of 4.8, 7.5, and 17.8 cm, and of 0.8-cm-wide Lego® bricks to heights of 8, 15, 30, and 45 cm. All walls spanned the full width of the tank. Barriers were placed at distances of 120, 180, and 240 cm from the source.

Runout position is measured as the maximum extent each current propagates along the floor of the tank. Liftoff position is measured as the forward edge of the first part of the current to rise buoyantly as a plume; in instances where plumes lift off in multiple locations, the farthest forward plume edge is measured. Note that this has the effect of biasing liftoff position downstream.

The relevant bulk and turbulent scaling parameters are defined in Table 1. Although the Reynolds numbers of our experiments are substantially lower than those of natural, dilute PDCs, the laboratory currents are fully turbulent and the other dimensionless numbers are similar to those of natural dilute PDCs (Burgisser et al., 2005); thus we are confident that the experiments accurately capture the large-scale dynamics of PDCs.

We estimate measurement uncertainties of <3% for U (mean current velocity), 10% for h (current thickness), <3% for m_c (current mass), and <0.2 °C for temperatures (T), corresponding

[1]GSA Data Repository item 2011331, experimental procedures, run conditions, and MPEG movies of experiments, is available online at www.geosociety.org/pubs/ft2011.htm, or on request from editing@geosociety.org or Documents Secretary, GSA, P.O. Box 9140, Boulder, CO 80301, USA.

to 17% for C_o (initial particle concentration), 0.05% for r_c (bulk current density), 17% for r_c/ρ, and 4% for D*T*. Energy densities have uncertainties of 15% for TE_b (buoyant thermal energy), and 17% for *KE* (kinetic energy); the ratio TE_b/KE has an uncertainty of 14%.

RESULTS

Movies of three experimental currents and a table of experiments are presented in the Data Repository. Laboratory density currents produced in our tank are typically 15–25 cm thick, have initial current head velocities of 10-20 cm/s, and densities of ~1.2–1.25 kg/m^3, corresponding to particle volume fractions of ~0.0007–0.003. Ambient density within the tank ranges from 1.18 to 1.23 kg/m^3. Current heads are typically ~60 cm long and form the thickest portions of the currents. Lobe and cleft structures are apparent in some currents as high-concentration regions that suddenly appear in the light sheet in front of the advancing head. The current heads are followed by tails with thicknesses typically two-thirds those of the heads. Variations in experiment duration do not noticeably affect the length of current heads, but affect the tails such that short-duration experiments generate currents composed almost entirely of the head, whereas longer duration currents have well-developed tails.

Large eddies generally form along the upper surfaces of the currents (Fig. 1). In currents with well-developed tails, those eddies grow from Kelvin-Helmholtz instabilities at the shear interface between the tails and ambient atmosphere. The first large eddies generally form on the rear of the current heads and often have streamwise length scales similar to *h* and heights of 0.2–0.5 *h*. Smaller eddies are occasionally visible at the noses of currents, suggesting minor air entrainment beneath the leading edges of currents. In flows that lift off, large eddies form on the margins of the rising plume.

Eddies form on the lower boundary of currents that transit and overshoot barriers before reattaching to the substrate (Fig. 1). Those structures are typically similar in size to those on the upper margins of currents. In some currents, plumes descend from the underside of currents as they pass over topography. Additional eddies often form on the upper surface of currents just upstream of the barriers (Fig. 1). Persistent circulations often develop to either side of barriers: on the upstream side, a large eddy forms between the wall and the detachment position as the current flows over the obstruction, and on the lee side between the barrier and reattachment point. Liftoff in these currents is typically focused near the barrier and not near the maximum runout position. When liftoff occurs, portions of the current downstream from the liftoff position reverse flow direction. During such reversals, current speed is similar in magnitude to the initial, downstream-directed flow.

Currents that encounter barriers greater in height than 1.5 *h* do not pass the obstructions and instead supply plumes above the barriers (Fig. 1).

TABLE 1. SCALING AND ENERGY DENSITIES OF NATURAL AND EXPERIMENTAL CURRENTS

	Natural PDCs	Experiments		Description
Re	10^6–10^9	10^3	$\frac{\rho_c U h}{\mu}$	Ratio of turbulent to viscous forces
Ri	0–10	0–20	$\frac{\Delta\rho g h}{\rho_{atm} U^2}$	Stratification stability
Ri_T	0–5	0–5	$\frac{g\Delta T \alpha h}{U^2}$	Ratio of buoyant to forced convection
Fr	~1	~1	$\frac{U}{\sqrt{g' h}}$	Inertial to gravitational forces
S_T	0.01–200	10^{-4}	$\frac{\tau_v(\rho_p - \rho_{atm})}{f\Lambda}\left(1+\frac{\rho_c}{2\rho_p}\right)$	Coupling of particles to turbulent motion
Σ_T	10^{-6}–10^5	<1	$\frac{u_r}{u'}$	Ratio of particle settling velocity to turbulent component of fluid velocity
KE	10^3–10^4 J/m^3	0.01–0.04 J/m^3	$\frac{\rho_c U^2}{2}$	Kinetic energy density
TE_b	10^3–10^4 J/m^3	0–0.2 J/m^3	$\rho_c \frac{C_{p,curr}}{C_{p,atm}} \alpha \Delta T g h$	Buoyant thermal energy density

Note: PDC—pyroclastic density currents. ρ_c and ρ_{atm} are the bulk current and atmospheric densities, $\Delta\rho$ is their difference, ρ_p is particle density; *U* and *u′* are the mean and turbulent velocities of the current; u_r is particle settling velocity; *g* and *g′* are gravity and reduced gravity; *h* is current thickness; Λ is the characteristic turbulent length scale; α is the coefficient of thermal expansion for air; $C_{p,curr}$ and $C_{p,atm}$ are the heat capacities of the bulk current and atmosphere; ΔT is the temperature difference between the current and atmosphere; τ_v is the characteristic particle response time; *f* is a drag coefficient. Values for natural PDCs are from Burgisser et al. (2005).

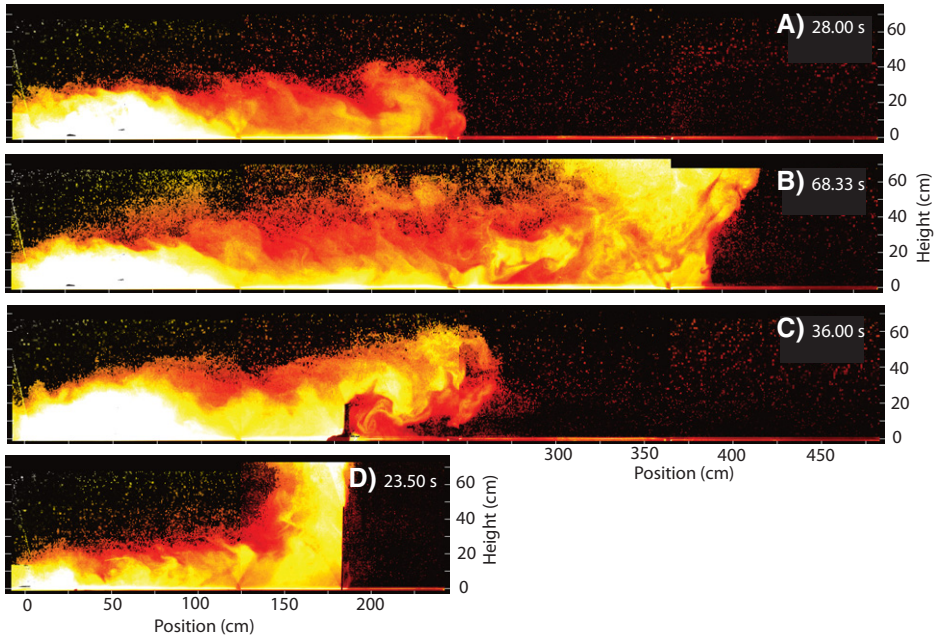

Figure 1. Images of experiments. A: As experiment 062510_3 travels across smooth floor of tank, head is well developed, and large eddies entrain air along top of current. B: Liftoff of experiment 062510_3 occurs near maximum runout position. C: Increased entrainment occurs beneath head of experiment 062510_3 as it surmounts 17.8 cm barrier; individual eddies even flow backward toward wall. D: Mean flow paths reorient vertically as 45 cm barrier blocks experiment 111910_2.

Runout Distance

To normalize the experimental runout distances and facilitate comparison with natural currents, we use the ratio, *D*, of the observed runout with that predicted by the ratio of current

speed and thickness to the Stokes settling velocity of the particles. Figure 2 summarizes the measurements and shows that runout decreases with increasing Richardson number, Ri, TE_b/KE, and Ri_T (not shown).

There is little correlation between runout distance and wall height in currents that traverse barriers with height <1.5 *h* (Fig. 2). Currents that encounter barriers ≥1.5 *h* do not overtop the walls, and thus runout terminates at the barrier. Topographic barriers thus exert a nonlinear control on runout where small walls have little to no effect, but larger barriers stop further propagation along the ground (Fig. 3).

There is no correlation between flow duration and *D*.

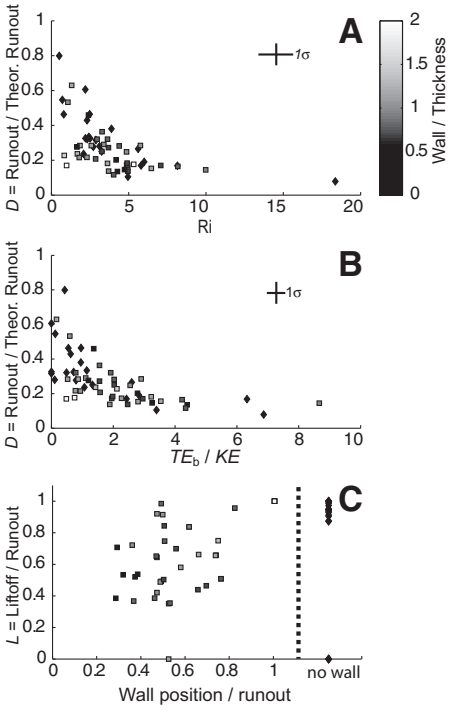

Figure 2. A: Runout, *D* (ratio of observed runout with that predicted by ratio of current speed and thickness to Stokes settling velocity of the particles), decreases with increasing Ri (Richardson number; see text) as faster currents are less stably stratified and entrain more air, but shows little dependence on barrier height (except for currents that encounter tall barriers). B: Hotter currents (high TE_b/KE) have shorter runout distances than cold currents. C: Liftoff, *L*, occurs near maximum runout position for currents traversing flat topography, but earlier in currents transiting barriers. Currents with liftoff plotting above 1:1 dash-dotted line exhibit complex liftoff that begins downstream of barrier before focusing above barrier. Currents traversing flat topography are indicated with diamond symbols; currents encountering barriers are plotted as squares; symbol color indicates ratio of wall height to current thickness. See text for definitions of variables.

Liftoff Position

Buoyancy reversals occurred, and buoyant plumes were generated, in nearly all experiments. Liftoff position decreases with TE_b/KE and follows three general behaviors. (1) In experiments traversing flat tanks, liftoff occurs near the maximum runout distance, and the ratio *L* of liftoff position and runout distance is typically >0.85. Once liftoff begins, the current tails feed directly into the rising plumes (Fig. 1). (2) Most experiments that traverse barriers generate buoyant plumes in the vicinity of the barriers, at *L* of 0.4–0.75 (Fig. 2). When liftoff begins, the portion of the current downstream from the liftoff position reverses direction and flows back toward the liftoff position (Fig. 3). A subset of currents that traverse barriers exhibits complex liftoff behavior where multiple plumes rise from the currents. In those experiments, liftoff results in the bulk of the current downstream of the barrier detaching from the base before flowing back and coalescing into a single dominant plume (often near the barrier). (3) Currents that encounter barriers with thickness >1.5 *h* do not traverse the barriers, but lift off at the barriers such that $L = 1$.

DISCUSSION

Controls on Runout Distance

The dominant controls on runout distance in our experiments are indicated by analysis of the Ri, TE_b/KE, and theoretical runout distance. Runout increases with current density and thickness, but decreases with increasing temperature. Those relations are not surprising given that denser, thicker currents travel faster and have greater particle concentrations requiring more time to sediment than smaller, more dilute currents. The effects of air entrainment on current mobility are negligible for currents with low Ri and thermal energy, as the resulting increases in current thickness are balanced by decreased density, but in higher temperature currents, air entrainment and expansion reduce the product of current density and thickness, thus runout decreases; these relationships are similar to those predicted by Bursik and Woods (1996) in their descriptions of subcritical and supercritical PDCs.

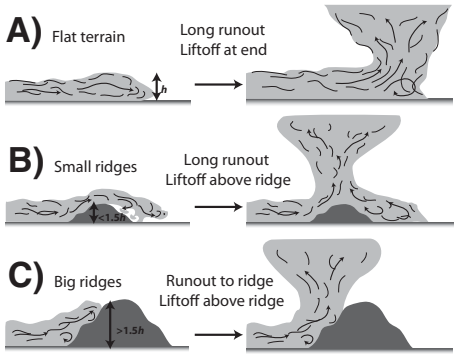

Figure 3. Effects of topography on runout, entrainment, and coignimbrite plume generation. A: Liftoff and runout are collocated in currents traversing flat topography. B: Currents that encounter barriers <1.5 *h* (*h* is current thickness) surmount obstructions and have runout similar to currents traversing flat topography. Overtopping barriers increases air entrainment and buoyancy near barriers, thus plumes focus above obstructions. As plumes rise, downstream portions of currents are drawn toward rising plume, generating local flow reversals. C: Barriers >1.5 *h* stop further propagation of currents and focus plumes when buoyancy reversals occur.

Runout distance is not significantly affected by either current duration or transit of topographic barriers (Fig. 3), highlighting two important and related aspects of current dynamics. First, properties of current heads control runout. Although runout is affected by current density, thickness, and thermal energy density, it does not vary with the total mass supplied to the currents, suggesting that the length of the tail is unimportant to runout. Second, that currents transiting barriers have runouts similar to those of currents that traverse flat terrain indicates that current heads overtop such barriers largely intact or are able to reform after reattaching to the substrate. This is important because enhanced entrainment is apparent in currents transiting barriers, particularly on the underside of the heads on the lee sides of barriers. Reconciling these apparently conflicting observations suggests that increased entrainment within current heads is volumetrically minor during transit of barriers, and regions of the head with increased entrainment are stripped from the heads as they pass the obstruction. When current heads reform, they are likely supplied by trailing portions of the current that did not undergo significantly enhanced entrainment.

The critical barrier height, h_{crit}, that discriminates between currents that transit barriers and those that do not is ~1.5 *h*. This value can be derived by converting kinetic energy to potential energy for currents with Froude numbers of 1. The 1.5 *h* critical height is less than that discussed by Simpson (1997), who described some spillover for barriers <2 *h*. The lower critical height in our experiments likely arises from increasing entrainment in portions of the current that start to spill over, resulting in liftoff (and thus termination of runout). Furthermore, those portions of the current that begin to spill over are likely less dense than the bulk current, and thus require less entrainment and expansion for buoyancy reversal.

Our experiments also suggest an important difference between dilute PDCs that undergo buoyancy reversal and other density currents. Woods et al. (1998) showed that blocking dilute

aqueous density currents produces an upstream-propagating bore that thickens the current until it overtops the obstruction. Because entrainment in those density currents leads to density reduction, but never buoyancy reversal, the currents can overtop barriers many times the current thickness. In contrast, although flow thickening occurs upstream of barriers in our experiments, bores are not apparent in most currents, and flow thickening leads to liftoff.

Controls on Liftoff Position

Liftoff occurs when currents have sedimented enough particles and entrained (and expanded) enough air that the current becomes less dense than the atmosphere (Woods and Kienle, 1994; Bursik and Woods, 1996). The liftoff position thus depends on how efficiently the current expands entrained air (proportional to the thermal energy density of the current) and the sedimentation rate of the current (which increases with particle settling velocity and decreases with increased thickness and turbulence intensity). Barring focusing of entrainment or sedimentation at a specific position, current density should systematically decrease with distance traveled (Dade and Huppert, 1996). In light of previous arguments suggesting that air entrainment is relatively minor in the current heads, we assume that within the heads, density is reduced primarily through sedimentation, whereas both entrainment and sedimentation operate within the tails.

When currents encounter barriers, liftoff occurs comparatively early and is often focused near the obstruction (Figs. 2 and 3). In currents encountering barriers <1.5 h, the current momentum is large enough to overtop the walls and the heads continue past the obstructions. As those heads transit the barriers, a large volume of air is trapped between the downstream side of the barrier and the overriding current; this volume of air is entrained and expanded by the current tail, resulting in enhanced mixing and earlier buoyancy reversal. The volume of air entrained on the lee side of the barriers should be strongly dependent on the slope of the lee side, with currents that surmount obstructions with gentle slopes entraining less air than currents that surmount and detach from steep barriers. Our experiments with vertical walls thus present the upper limit of increased entrainment. Once the current (tail) begins to lift off, more dilute and less dense portions of the current are drawn upward with the rising fluid, leading to plume formation. Tall barriers block currents, effectively setting the runout distance. Because density decreases during transport, the lowest densities should be near the runout distance, thus plumes will be focused near the obstruction. Regardless of barrier height, continuity dictates that the flow is redirected, at least partially, upward to overtop any barrier in the path of a current. Upward-directed flow near the barriers tends to focus the plumes at those locations.

SUMMARY

Our experiments suggest that dilute PDC runout is controlled by behavior of the current head, but liftoff and coignimbrite generation are strongly influenced by the current tails. The behavior of PDCs is strongly affected by interactions with topography of similar height to current thickness (Fig. 3). That experimental currents surmount barriers to 1.5 h indicates that PDCs should also overtop ridges with relief of as much as 1.5 h; this relationship provides a means of estimating minimum current thickness based upon maximum topographic relief between volcanic vents and distal PDC deposits. Considering that even small-volume PDCs can have thicknesses of hundreds of meters (Woods and Kienle, 1994; Fujii and Nakada, 1999), these results suggest that dilute PDCs should overtop ridges with >200 m relief. Topographic obstructions large enough to arrest flow propagation will focus plume development, but even smaller barriers increase air entrainment sufficiently to provide a focus for plumes. In PDCs that do not traverse barriers, plume formation should occur near the runout position.

ACKNOWLEDGMENTS

William Gange provided assistance running many experiments. Stuart Foster helped build the experimental apparatus. Bill Dietrich and Leonard Sklar provided space at the Richmond Field Station. Andrews was supported by a National Science Foundation (NSF) Earth Sciences Postdoctoral Fellowship (EAR-0847366). Manga was supported by NSF grant EAR-080954. Thoughtful comments by G. Valentine, A. Burgisser, and one anonymous reviewer helped improve this paper.

REFERENCES CITED

Burgisser, A., Bergantz, G.W., and Breidenthal, R.E., 2005, Addressing the complexity in laboratory experiments: The scaling of dilute multiphase flows in magmatic systems: Journal of Volcanology and Geothermal Research, v. 141, p. 245–265, doi:10.1016/j.jvolgeores.2004.11.001.

Bursik, M.I., and Woods, A.W., 1996, The dynamics and thermodynamics of large ash flows: Bulletin of Volcanology, v. 58, p. 175–193, doi:10.1007/s004450050134.

Bursik, M.I., and Woods, A.W., 2000, The effects of topography on sedimentation from particle-laden turbulent density currents: Journal of Sedimentary Research, v. 70, p. 53–63, doi:10.1306/2DC408FE-0E47-11D7-8643000102C1865D.

Bursik, M.I., Kurbatov, A.V., Sheridan, M.F., and Woods, A.W., 1998, Transport and deposition in the May 18, 1980, Mount St. Helens blast flow: Geology, v. 26, p. 155–158, doi:10.1130/0091-7613(1998)026<0155:TADITM>2.3.CO;2.

Calder, E.S., Sparks, R.S.J., and Gardeweg, M.C., 2000, Erosion, transport and segregation of pumice and lithic clasts inferred from ignimbrite at Lascar Volcano, Chile: Journal of Volcanology and Geothermal Research, v. 104, p. 201–235, doi:10.1016/S0377-0273(00)00207-9.

Criswell, W., 1987, Chronology and pyroclastic stratigraphy of the May 18, 1980, eruption of Mount St. Helens, Washington: Journal of Geophysical Research, v. 92, p. 10237–10266, doi:10.1029/JB092iB10p10237.

Dade, W.B., and Huppert, H.E., 1996, Emplacement of the Taupo ignimbrite by a dilute turbulent flow: Nature, v. 381, p. 509–512, doi:10.1038/381509a0.

Doronzo, M.D., Valentine, G.A., Dellino, P., and de Tullio, M.D., 2010, Numerical analysis of the effect of topography on deposition from dilute pyroclastic density currents: Earth and Planetary Science Letters, v. 300, p. 164-173, doi:10.1016/j.epsl.2010.10.003

Dufek, J., and Bergantz, G.W., 2007, Suspended load and bed-load transport of particle-laden gravity currents: The role of particle-bed interaction: Theoretical and Computational Fluid Dynamics, v. 21, p. 119–145, doi:10.1007/s00162-007-0041-6.

Fisher, R.V., Orsi, G., Ort, M.H., and Heiken, G., 1993, Mobility of a large-volume pyroclastic flow—Emplacement of the Campanian ignimbrite, Italy: Journal of Volcanology and Geothermal Research, v. 56, p. 205–220, doi:10.1016/0377-0273(93)90017-L.

Fujii, T., and Nakada, S., 1999, The 15 September 1991 pyroclastic flows at Unzen Volcano (Japan): A flow model for associated ash-cloud surges: Journal of Volcanology and Geothermal Research, v. 89, p. 159–172, doi:10.1016/S0377-0273(98)00130-9.

Gardner, J.E., Burgisser, A., and Stelling, P., 2007, Eruption and deposition of the Fisher Tuff (Alaska): Evidence for the evolution of pyroclastic flows: Journal of Geology, v. 115, p. 417–435, doi:10.1086/518050.

Miller, T.P., and Smith, R.L., 1977, Spectacular mobility of ash flows around Aniakchak and Fisher Calderas, Alaska: Geology, v. 5, p. 173–176, doi:10.1130/0091-7613(1977)5<173:SMOAFA>2.0.CO;2.

Simpson, J.E., 1997, Gravity currents in the environment and the laboratory (second edition): Cambridge, Cambridge University Press, 244 p.

Wilson, C.J.N., 2008, Supereruptions and supervolcanoes: Processes and products: Elements, v. 4, p. 29–34, doi:10.2113/GSELEMENTS.4.1.29.

Woods, A.W., and Kienle, J., 1994, The dynamics and thermodynamics of volcanic clouds: Theory and observations from the April 15 and April 21, 1990 eruptions of Redoubt Volcano, Alaska: Journal of Volcanology and Geothermal Research, v. 62, p. 273–299, doi:10.1016/0377-0273(94)90037-X.

Woods, A.W., Bursik, M.I., and Kurbatov, A.V., 1998, The interaction of ash flows with ridges: Bulletin of Volcanology, v. 60, p. 38–51, doi:10.1007/s004450050215.

Manuscript received 3 March 2011
Revised manuscript received 21 June 2011
Manuscript accepted 27 June 2011

Printed in USA